RGNZ/MGPB

Impacts of Ammonium Sulfate Leaching on Ion Adsorption Rare Earths and Soil Mechanical Properties

Rudarsko-geološko-naftni zbornik
(The Mining-Geology-Petroleum Engineering Bulletin)
UDC: 622.7
DOI: 10.17794/rgn.2024.1.3

Preliminary communication

Amirul Asyraf Mohd Hamka[1]; Meisam Saleki [2]; Zohreh Nabavi[3]; Hesam Dehghani[4]

[1] School of Materials and Mineral Resources Engineering, Engineering Campus, Universiti Sains Malaysia 14300 Nibong Tebal, Pulau Pinang, Malaysia

[2] School of Materials and Mineral Resources Engineering, Engineering Campus, Universiti Sains Malaysia 14300 Nibong Tebal, Pulau Pinang, Malaysia, ORCID: https://orcid.org/0000-0001-5858-3948

[3] Department of Mining Engineering, Faculty of Engineering, Tarbiat Modares University, Tehran, Iran, ORCID: https://orcid.org/0009-0009-6513-7941

[4] Mining Engineering Faculty, Hamedan University of Technology, Hamedan, Iran, ORCID: https://orcid.org/0000-0003-2029-9540

Abstract

In-situ leaching (ISL) has gained prominence as a non-destructive method for rare earth element (REE) extraction, particularly in regions like China. However, concerns over the environmental impact and soil stability due to ISL activities have surfaced following a landslide incident. This article distills the essence of a comprehensive research endeavor that delves into the effects of ammonium sulfate ISL leaching, employing concentrations of 0.05M, 0.1M, and 0.5M, on soil mechanical properties. The study encompasses physicochemical, physical, and mechanical tests, unveiling substantial alterations in shear strength, cohesion, angle of internal friction, zeta potential, liquid limit, plastic limit, and plasticity index following leaching. XRF and XRD analyses reveal the presence of REEs and distinctive mineral phases in the soil samples. Overall, ISL induces a weakening of the soil, raising concerns about potential slope failures and emphasizing the need for a deeper understanding of ISL's impact on soil properties in the context of REE mining.

Keywords:
in-situ leaching (ISL); soil mechanical properties; rare earth elements (REEs); ammonium sulfate leaching; environmental impact

1. Introduction

Ion-absorbed rare-earth deposits are a distinctive mineral resource containing an abundance of medium-heavy rare-earth elements. These valuable deposits have been found in various geographic regions across the globe, with a particular concentration in southern China (**Borst et al., 2020; Dushyantha et al., 2020; Stockdale and Banwart, 2021**). Following extended weathering of granite or volcanic rocks containing rare-earth elements, ion-absorbed rare-earth deposits eventually degrade into a soil enriched with these valuable elements (**Deng et al., 2019; Fu et al., 2019; Yang et al., 2019**). In this particular deposit, rare-earth elements are found by adhering to clay minerals within the weathering layer, mainly as dehydrated cations or hydroxyl hydrous cations. Consequently, rare-earth ions can be readily removed from this context by ion exchange using an electrolyte solution with a specific concentration (**Moldoveanu and Papangelakis, 2012, 2013; Stockdale and Banwart, 2021; Yang et al., 2018**).

Corresponding author: Meisam Saleki
e-mail address: meisam.saleki@gmail.com

Ion-absorbed rare-earth ores have seen three different mining methods employed across generations: vat leaching, heap leaching, and in-situ leaching (**Yang et al., 2013; Zhang et al., 2016**). At present, in-situ leaching is the predominant method for extracting rare-earth resources, and the leaching agents have transitioned from sodium chloride to the more commonly utilized ammonium sulfate solution (**Huang et al., 2015; Nie et al., 2020; Zhang et al., 2016**). The leaching process operates under the assumption that a substantial volume of electrolyte solution is consistently introduced into the rare-earth ore body. Within this process, cations from the electrolyte solution replace rare-earth ions. Subsequently, the desorbed rare-earth ions within the solution migrate to one side of the collection channel, where they accumulate in a reservoir, creating a solution enriched with rare-earth elements. Relative to the earlier two generations of leaching methods, in-situ leaching offers advantages such as reduced project duration, decreased construction expenses, consistently high recovery rates for rare-earth elements, and environmental preservation, making it a favorable choice (**Huang et al., 2015; Nabavi et al., 2023a**). The survey findings suggest that ongoing agent injection alters the physical and mechanical

characteristics of rare-earth ores, diminishing or undermining their utility in engineering applications (**Kazemi et al., 2023a; Yang et al., 2013; Zhang et al., 2016**). To ensure the secure and efficient extraction of rare-earth resources, it's essential to comprehend the mechanical properties and workings of the rare-earth ore body during the leaching procedure.

Ion-absorbed rare-earth ores, existing as weathered soil, possess a porous structure consisting of sand, silt, and clay, with a significant quantity of fine particles measuring less than 75 μm within the weathered layer (**Chen, Zhang, Liu, et al., 2020**). As a result, alterations in both the physical and chemical parameters have the capability to exert an influence on the soil's shear strength (**Chen et al., 2023; Chen, Zhang, and Chi, 2020; Guo et al., 2022**).

ISL is widely used for uranium mining, as well as for copper and other metals. ISL has some advantages over conventional mining methods, such as lower cost, less surface disturbance, and reduced waste generation. However, ISL also poses some environmental challenges and risks, such as groundwater contamination, aquifer restoration, and ecological impacts. Therefore, ISL requires careful assessment and monitoring of its potential environmental impacts, as well as mitigation and remediation measures to protect human health and the environment (**Agency, 2005; Nabavi et al., 2023b**).

In the past few years, there has been a significant amount of research aimed at examining how water and chemical solutions impact the macro-structural, physical, and mechanical properties of rock materials (**Asahina et al., 2018; Dieterich and Conrad, 1984; Feng et al., 2004; Hampton et al., 2018; He et al., 2021; Kazemi et al., 2023b; Kazemi et al., 2023c; Li et al., 2014; H. Li et al., 2020; M. Li et al., 2020; Lin et al., 2020; Miao et al., 2016; Shang et al., 2020; Shu et al., 2019; Wang et al., 2018; Yu et al., 2020**). For instance, **Xie et al. (2011)** examined alterations in the mechanical attributes of porous limestone materials caused by chemical solution erosion. Their experimental findings indicated that the chemical corrosion led to a partial decrease in the pore collapse limit stress, elastic modulus, and cohesion of the rock specimen. **Izadi and Elsworth (2015)** researched the permeability traits and failure mechanisms of rocks when subjected to thermal, hydraulic, mechanical, and chemical interactions, employing FLAC3D models. **H. Li et al. (2020)** examined the chemical interaction between the acidic solution and the primary diagenetic mineral constituents within the sandstone sample, approaching it from a chemical kinetics standpoint. **Lin et al. (2020)** utilized nuclear magnetic resonance (NMR) methodology to assess changes in porosity and variations in pore size distribution features in sandstone samples submerged in chemical solutions of varying pH levels. They deliberated on the erosion process affecting sandstone when exposed to acidic solutions. **Wang et al. (2020)** conducted a comparison of the permeability of rare-earth ore samples while subjecting them to the leaching process with water and ammonium sulfate. The findings indicate that the permeability coefficient of the ore samples remained consistent throughout the entire water leaching process, whereas it exhibited a notable decrease during ammonium sulfate leaching before stabilizing until the completion of the leaching.

Zhong et al. (2022) conducted laboratory tests to investigate the erosion effects of leaching solutions on basement rock in ion-adsorbed rare earth deposits. Their study uncovers significant reductions in rock strength, mass, and P-wave velocity, alongside heightened porosity and a changing failure pattern, providing critical insights into the evolution characteristics of leaching solution-induced damage in the context of in situ leaching mining. **Wang et al. (2023a)** have undertaken a comprehensive investigation into the recovery of rare earth resources from weathered crust elution-deposited rare earth ore (WCEDRE-ore). Their work unveils the intricate relationship between ammonium sulfate leaching and the alteration of engineering properties, emphasizing the pivotal role of soil-water chemical reactions, ion exchange, and pore structure transformations in determining the success of the in situ leaching process for WCEDRE-ore. **Wang et al. (2023b)** comprehensively investigate the impact of leaching on the microstructural characteristics of ion-adsorbed rare earth ore samples. Their study leverages advanced techniques, including scanning electron microscopy (SEM) and nuclear magnetic resonance (NMR), to elucidate the intricate relationship between the evolving microstructure and the mechanical properties of these ores, shedding new light on the mechanism behind shear strength parameter weakening during the leaching process. **Feng et al. (2023)** explored the utilization of a compound leaching agent, combining ammonium sulfate and ammonium formate, to mitigate challenges in the leaching process of weathered crust elution-deposited rare earth ore. Their study yielded notable enhancements in rare earth mass transfer efficiency while effectively curbing aluminum transfer, suggesting a promising approach for more efficient and eco-friendly rare earth extraction.

This research endeavors to delve into the alteration of mechanical properties in soil samples induced by the ammonium sulfate IAC leaching of various concentrations. Employing a comprehensive methodology that encompasses column leaching tests, direct shear box tests, XRD, XRF, zeta potential, and liquid and plastic limit test, this study yields invaluable insight into modifications occurring during leaching. The findings of this research are poised to serve as a scientific cornerstone for the optimization of future leaching processes and the prevention of associated risks.

2. Materials and methods

2.1 Experimental process

Unaltered ore soils possess a loose composition with limited cohesion, making them unsuitable for maintaining

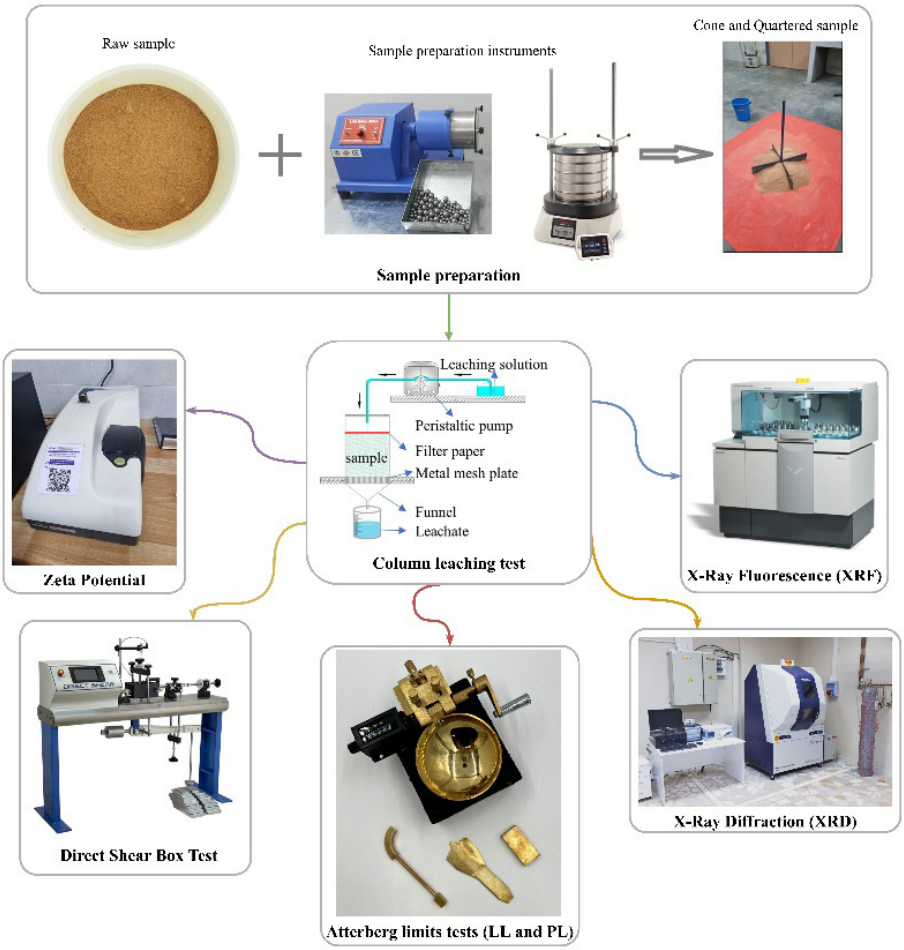

Figure 1: Diagram outlining the testing process

their integrity during transportation. Hence, to create standardized test samples, the gathered soil specimens were reconfigured and employed in subsequent testing. Various experimental techniques were employed to study the weakening process of the rare-earth ore body due to ion absorption during leaching, as illustrated in **Figure 1**.

Initially, the sample underwent a drying process in an oven and was subsequently homogenized using a ball mill. Following homogenization, the sample underwent separation through cone and quartering, leading to division into four bags: one for the initial state before leaching and three for varying concentrations of ammonium sulfate post-leaching. Subsequently, only the first sample underwent a series of three different testing methods encompassing physicochemical, physical, and mechanical evaluations. Concurrently, the remaining three samples underwent the leaching process, with the leached samples subsequently being dried for 24 hours. Once dried, all samples underwent the comprehensive battery of testing methods to assess their physicochemical, physical, and mechanical properties.

2.2 Soil samples and physical properties

This study involved laboratory experiments to examine how the leaching solution affected the mechanical characteristics of ion-adsorbed rare earth deposit soils. The soil samples for this study were acquired from a rare-earth mine with ion-adsorption characteristics in Kelantan, through collaboration with a mineral resources' lecturer at USM.

The sample was positioned on a canvas, which was then gently stretched from both sides to create a cone shape. To ensure homogeneity, the cone was divided into four equal sections using a metal divider, as illustrated in **Figure 1**. This process was iterated three times to guarantee the attainment of a uniformly mixed sample. Subsequently, each section was carefully transferred into individual buckets, designated for subsequent experiments. One bucket held the sample before the leaching process, while the remaining three were allocated for the leaching process, to be conducted thrice with distinct settings.

Following the Chinese geotechnical test standard GB/T 50123–2019 (**Cai et al., 2019**), the particle size distribution of soil particles larger than 75 μm was determined using the sieving technique. This involved employing a set of sieves, with all samples weighed, including the material collected in the pan. **Figure 2** illustrates that the calculated uniformity coefficient (Cu) for the tested soil's particle size distribution was 6.419, and the

curvature coefficient (Cc) was measured at 0.645. Therefore, based on both Cu and Cc values, we can conclude that the soil is not well-graded and has a poor mixture of different particle sizes. Furthermore, **Table 1** presents the physical characteristics of undisturbed rare-earth ore samples, encompassing details such as particle size distribution, cohesion, internal friction angle, and moisture content.

The soil's mineral composition was assessed through X-ray diffraction (XRD) tests, as depicted in **Figure 3**.

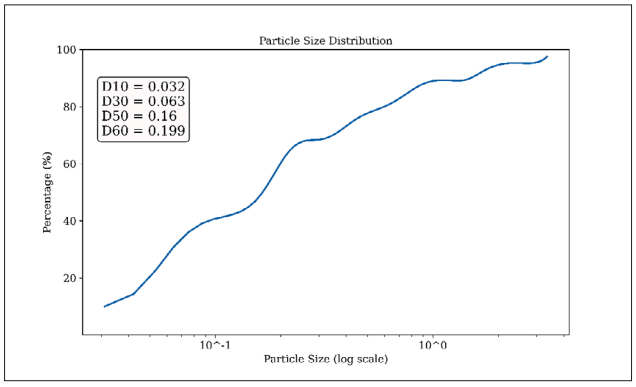

Figure 2: Soil particle size distribution curve

The XRD results revealed that the predominant components of the collected soil were Illite, Indium Yttrium Antimony Sulfide, and Thulium Thorium Iodide. The peak with the highest intensity in the X-ray diffraction (XRD) analysis corresponded to Indium Yttrium Antimony Sulfide. Additionally, the X-ray fluorescence (XRF) analysis revealed the presence of Y_2O_3, which was distinctive compared to other rare-earth elements (REEs). Other potential REEs identified included Thulium, Thorium, and Illite, a clay mineral bearing REEs. Although the Yttrium percentage in the XRF analysis was relatively low in comparison to other compounds, it was the sole REE present in a notable quantity. Moreover, most of the prominent peaks in the XRD graph were associated with Indium Yttrium Antimony Sulfide.

In addition, **Table 2** presents the ore sample's chemical composition, determined using X-ray Fluorescence (Axios max, PANalytical B.V.). Notably, the analysis revealed that Sc_2O_3 (0.0020%) and Y_2O_3 (0.0280%) had the highest concentrations among the chemical constituents. However, the quantity of rare-earth elements in the sample was relatively limited, indicating the need for a systematic and precise leaching process to extract as many REEs as possible.

Table 1: Physical characteristics of Kelantan rare-earth ore samples

Parameters	Cohesion (kPa)	Angle of internal friction (°)	Moisture content (%)	Distribution in particle size (mm)		
				D25	D50	D75
Value	4.3	38.65	27	0.057	0.16	0.43

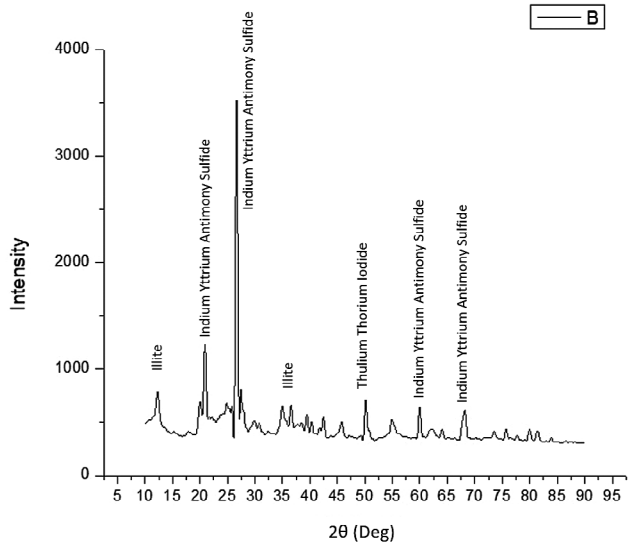

Figure 3: XRD spectrum of the soil

Table 2: XRF findings for original samples

Compound	Compound Unit	Element
Sc2O3	0.0020%	0.0013%
Y2O3	0.0280%	0.0220%

2.3 The leaching solution

The mineralization characteristics of ion-adsorbed rare earth minerals are unique, with rare earth ions primarily adhering to the surface of clay minerals in hydrated or hydroxyl-hydrated forms. As a result, various electrolytes can serve as leaching solutions **Wang et al. (2020)**. To balance cost and efficiency, most ion-adsorbed rare earth ore extraction processes use in-situ entry and exit methods, employing ammonium sulfate as the preferred leaching agent. For the leaching experiment, a column leaching approach will be employed. Approximately 700g of ion-adsorption clay will be packed into a glass leaching column, equipped with a sand core filter at the base and a filter paper at the top. The leaching will occur at room temperature, with ammonium sulfate solutions at concentrations of 0.05M, 0.5M, and 2.5M. The experimental setup is detailed in **Figure 4**.

2.4. Direct Shear Box Test

To conduct the Direct Shear Box Test, the initial step involved homogenizing the sample and reducing its size with a ball mill over a five-minute duration. Following

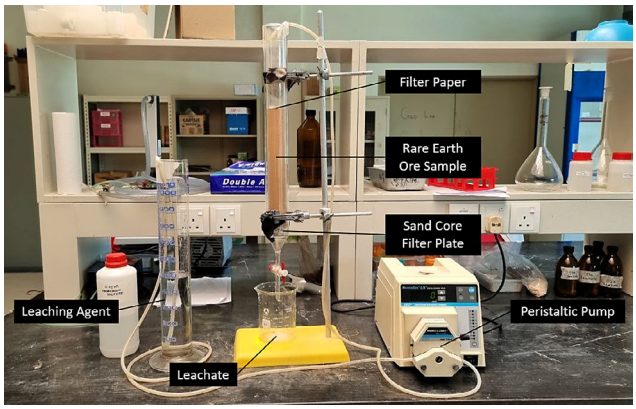

Figure 4: Column leaching device

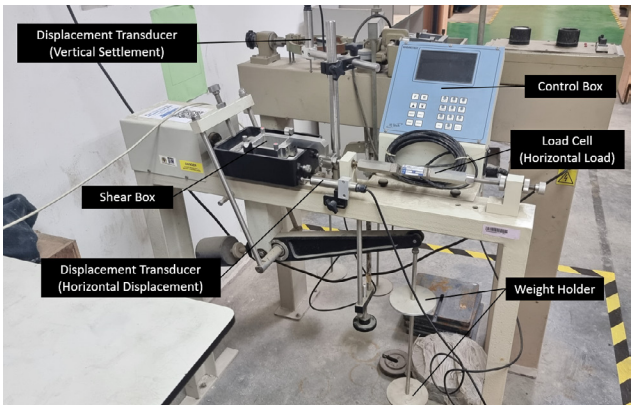

Figure 5: Shear box setup and configuration

this, the sample was sieved using a 1 mm sieve, retaining the passed portion for the experiment.

The setup process began with measuring the dimensions of the shear box, and the apparatus was assembled according to the configuration shown in **Figure 5**. A normal load of 20kg was selected for the initial run. The shear box components were placed within the direct shear box machine, and the depth of the shear box was established. Subsequently, the shear box was weighed using an electronic balance. The sample was carefully placed inside the shear box and compacted, and the mass of the sample was recorded by reweighing the shear box. The distance from the top of the sample was measured, and a dial gauge was positioned to measure shear and normal displacements. These settings were managed through a computer interface, and initial readings for both dial gauges were documented. The wheel was rotated at two revolutions per minute, and readings for all three dial gauges were recorded every 10 seconds. The test was concluded when readings showed five consecutive declines. This process was then repeated using a new sample, with the normal load adjusted to 30kg and 40kg, respectively. Ultimately, three graphs were constructed to determine the angle of friction and cohesion.

2.5. Zeta Potential

The test involves measuring the velocity of charged particles as they move under the influence of an electric field. The procedure began by filling a 100mL beaker with ultrapure water, into which a glass stirring rod was introduced and stirred with the soil sample. The beaker was sealed with parafilm and partially submerged in an ultrasonic bath for five minutes, followed by a five-minute rest. A few mL of the solution was extracted using a syringe from the surface layer of the beaker's solution. The folded capillary cell's protective cap was removed, and the cell was inverted with the syringe attached to one end. The solution was gradually injected until it reached the midline, after which the cell was repositioned upright, and the injection continued until the cell was full, ensuring no air bubbles were present. The capillary cell was then sealed with protective caps on each end, and the Zetasizer instrument was prepared by closing its cover and confirming the yellow LED was illuminated. The zeta potential software was operated via a computer.

2.6. Liquid Limit Test

The liquid limit test, a key soil mechanics procedure for establishing a soil's liquid limit, was conducted using the cone penetrometer test method. The process involved several steps: After passing a dried soil sample through a 425-micron sieve, 150 grams of the soil were weighed. Distilled water was measured using a graduated cylinder to ensure precise water measurement. The soil and water were thoroughly mixed until a uniform paste formed, then transferred to a metal cup. The paste was tamped down to align with the cup's top using a wooden mallet. The cone penetrometer apparatus was set up, with the cone tip positioned directly above the paste. The stopwatch was initiated, and the cone penetrometer was released; after five seconds, the stopwatch was halted, and the cone penetration depth was recorded. This process was repeated four more times. A small amount of the soil paste was collected and dried in an oven for 24 hours at 100°C to ascertain the moisture content.

2.7. Plastic Limit Test

The plastic limit test, a soil mechanics assessment determining a soil's plastic limit or the water concentration at which it shifts from a plastic to a semisolid state, involved several steps. The sample underwent sieving with a 75-micron sieve after 24 hours of oven drying. Approximately 200g of the sample was then weighed. The sample was placed in a mixing can, and distilled water was gradually added and thoroughly mixed with a spatula to achieve homogeneity. The wet soil was rolled on a glass plate using the palm until a 5 mm diameter thread formed. This rolling process was repeated until the soil began to break apart when reaching the 5 mm diameter size. The soil was divided into five smaller threads, placed in moisture cans, and dried for 24 hours in an oven. Weights were recorded for empty moisture

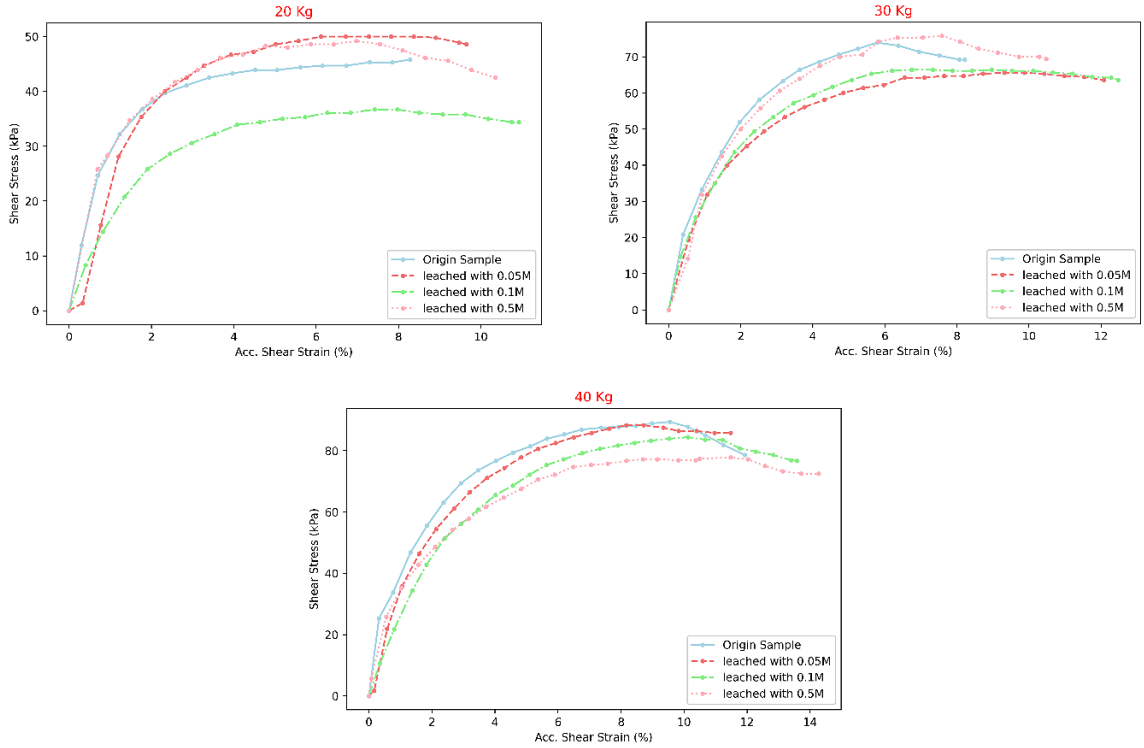

Figure 6: Shear box test results

cans, moisture cans with wet soil, and moisture cans with dried soil, enabling the calculation of the soil's water content and subsequently, the plastic limit.

2.8. X-Ray Diffraction (XRD)

X-ray diffraction (XRD), a non-destructive analytical method, is employed to reveal the crystalline structure and phase composition of materials. To prepare the sample, it underwent five cycles of 10-second milling to achieve a target size of 75 microns and was subsequently sieved through a 75-micron sieve. Fifteen grams of the sample were placed in a bag and sent to the XRD laboratory for further analysis. The scanning angle ranged from 0° to 90°. The X'Pert HighScore Plus software was utilized to identify pattern peaks in each sample, and the data was re-plotted using Origin-Pro. To identify the phases present in the sample, the XRD patterns were compared to the International Centre of Diffraction Data (ICDD) files.

2.9. X-Ray Fluorescence (XRF)

X-ray fluorescence (XRF) is a non-destructive analytical method used to ascertain the elemental composition of a material. Sample preparation involved subjecting the sample to five cycles of 10-second milling to attain the desired 75-micron size, followed by sieving through a 75-micron sieve. Fifteen grams of the sample were then placed in a bag and sent to the XRF laboratory for further analysis. The results, expressed as percentages of the desired elements, were readily interpretable. A comparative analysis of each element was performed for all four samples.

3. Experimental Results and Analysis

3.1. Direct Shear Box Test Analysis of Leached Samples

In this section, we delve into the comprehensive analysis of soil samples to evaluate the mechanical properties, focusing on the effects of leaching. The direct shear box tests offer valuable insight into the soil's behaviour and shear strength before and after undergoing leaching processes.

Figure 6 portrays the outcomes of direct shear box tests conducted on soil samples including of origin, leached with 0.05M, leached with 0.1M, and leached with 0.5M. These tests vary the normal load, with weights of 20kg, 30kg, and 40kg. In **Figure 6**, the applied normal loads were 196.2k for 20kg, 294.3kN for 30kg, and 392.4kN for 40kg. The x-axis represents accumulative shear strain, while the y-axis reflects shear stress. As anticipated, the graph exhibits an expected pattern, with the highest weight of 40kg yielding the highest results, and the lowest weight of 20kg producing the lowest values.

The resultant graphs display a predictable trend: higher weights lead to greater shear stress. This is attributed to increased vertical force causing more soil compac-

tion, thus enabling the soil to withstand higher shear stress before failing.

3.1.1. Shear Stress

Table 3 offers a comparative analysis of shear stress values, considering different normal stresses and leaching conditions. The comparison involves the original sample and three samples leached using 0.05M, 0.1M, and 0.5M ammonium sulfate. For the first normal stress of 54.50 kPa, shear stress values exhibit inconsistency without a clear pattern, which contradicts the anticipated reduction in shear stress after leaching. The second normal stress of 81.75 kPa presents more consistent shear stress values for the leached samples, except for the 0.5M sample, which displayed a higher shear stress, possibly due to compaction issues. The final normal stress of 109.00 kPa yields consistent and decreasing shear stress values below the original sample. The higher normal stress applied is likely the reason for this consistency, preventing voids and ensuring more reliable readings.

Table 3: Comparison in shear stress values

Normal Stress (kPa)	Shear Stress (kPa)			
	0M	0.05M	0.1M	0.5M
54.50	45.8	50	36.7	49.2
81.75	73.9	65.6	66.4	75.8
109.00	89.4	88.3	84.4	77.8

Figure 7 presents a histogram that enhances the clarity of shear stress value comparisons. The variation in shear stress, particularly at higher normal stress levels, offers valuable insight into the soil's subsurface characteristics. While the stress may not significantly differ from the site's conditions, this data provides a glimpse into how leaching activities impact the soil's shear strength, particularly in the lower soil layers.

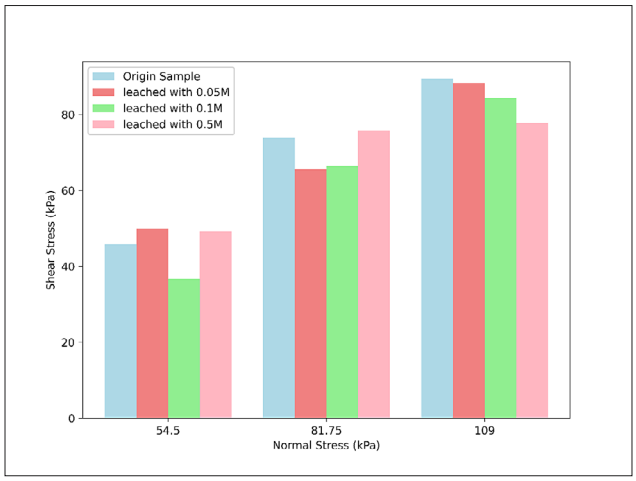

Figure 7: Comparison between shear stress values

3.1.2. Cohesion

Table 4 provides an overview of the cohesion values observed in the various samples. The original sample exhibited a relatively low cohesion value. However, a distinctive trend was observed in the leached samples, starting at 10.52 kPa for 0.05M and reaching 24.70 kPa for 0.5M. It's important to note that the cohesion value for the 0.1M sample appears as negative, which is inconsistent with expected behaviour, as cohesion values cannot be negative.

Table 4: Cohesion values for samples

Concentration (M)	Cohesion (kPa)
Original	4.30
0.05	10.52
0.1	-9.05
0.5	24.70

This seemingly anomalous result can be attributed to the negatively charged nature of the soil, a characteristic determined by zeta potential measurements. The presence of ammonium ions introduced during the leaching process may have promoted flocculation, a process that leads to the aggregation of soil particles and improved soil structure. As a consequence, this enhancement in soil structure likely contributed to an increase in cohesion. Therefore, it is evident that as the concentration of ammonium sulfate in the leaching solution increased, the cohesion values also exhibited a corresponding increase. This observation underscores the influence of leaching conditions on the cohesion properties of the soil.

3.1.3. Angle of Internal Friction

The angle of internal friction (φ) is a measure of the resistance of a soil to shear stress. It depends on the shape, size, and arrangement of the soil particles, as well as the moisture content and density of the soil. The angle of internal friction can be determined by conducting laboratory tests, such as the direct shear test or the triaxial test, on a soil sample. The tests involve applying different combinations of normal and shear stresses on the sample and measuring the resulting deformation and failure. The angle of internal friction can be calculated by plotting the shear stress versus the normal effective stress on a graph and finding the angle of the line that best fits the data points. The angle of internal friction is usually expressed in degrees. For example, in 0.1M samples, the equation was:

$$y = 0.8752x - 9.05 \quad (1)$$

Where:

y - represents the shear stress (kPa),

x - represents the normal effective stress (kPa).

The y-intercept is the cohesion, minimum shear stress that been applied to sample prior to starting the experiment, when the normal stress is zero, which is -9.05 kPa. The gradient is the friction angle, and when convert to phi, it is 41.19°.

Figure 8 presents a histogram illustrating the variations in the friction angle values. An anticipated decrease in the friction angle was observed with increasing concentrations of the leaching reagent. This phenomenon may be attributed to the presence of ammonium ions, which can potentially disrupt interparticle bonds, leading to weaker interparticle interactions.

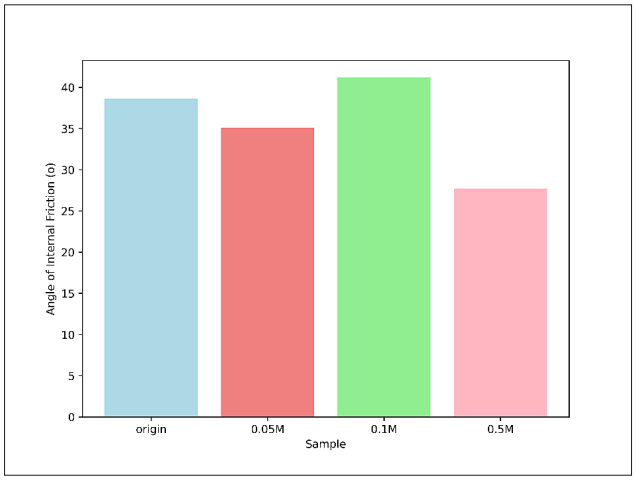

Figure 8: Comparison of angle of internal friction

Moreover, the reduction in fine content resulting from the leaching process may also contribute to the decline in the angle of internal friction with increasing concentrations, a phenomenon suggested by previous research (**Saadatkhah et al., 2023**). The consistency of this trend was evident in the 0.05M and 0.5M samples. However, it's worth noting that the 0.1M sample exhibited values that could be considered outliers, much like the anomalous results in cohesion. An instrumental or procedural error during the shear box test for the 0.1M sample may have impacted the overall values of shear stress, consequently affecting the measured shear strength, cohesion, and angle of internal friction.

3.2. XRF Analysis of Leached Samples

Following the application of different concentrations of ammonium sulfate for leaching, an X-ray fluorescence (XRF) analysis was conducted to evaluate the impact on rare earth element (REE) concentrations in the soil samples. This analysis revealed distinct patterns for each leached sample. To gain a comprehensive understanding of the leaching process's influence on REE concentrations, a comparative analysis was conducted. The comparison was made between the original sample and the leached samples, as presented in **Table 5**. Notably, the results uncovered unique insight into potential detection limits and variations in leaching efficiency.

Table 5: XRF comparative analysis of different samples

Element	Scandium (Sc)	Yttrium (Y)	Ytterbium (Yb)
Original	0.0013%	0.0220%	-
0.05M	-	0.0197%	-
0.1M	-	-	-
0.5M	0.0264%	-	0.0019%

For the 0.05M ammonium sulfate leaching, as shown in **Table 5**, the concentration of Yttrium (Y) decreased to 0.0197%, which is notably lower than the pre-leaching sample. In contrast, the 0.1M ammonium sulfate leaching, displayed in **Table 5**, resulted in an absence of detectable REEs in the sample, possibly due to the low initial REE concentration. Conversely, when subjected to 0.5M ammonium sulfate leaching, the soil sample exhibited increased Scandium (Sc) and Ytterbium (Yb) concentrations, reaching 0.0264% and 0.0019%, respectively.

In this comparative analysis, it was evident that some REEs experienced changes in concentration due to the leaching process. For instance, the concentration of Scandium (Sc) in the 0.5M leached sample increased from 0.0013% to 0.0264%. Conversely, the value of Yttrium (Y) decreased in the 0.05M leached sample, possibly indicating successful leaching. However, Y was not detectable in both the 0.1M and 0.5M leached samples. Lastly, for Ytterbium (Yb) in the 0.5M leached sample, the value was already very low, and it may not have been detected by the XRF machine in the previous testing of the original sample, 0.05M sample, and the 0.1M sample.

In the 0.05M ammonium sulfate leaching, the decrease in Yttrium (Y) concentration to 0.0197% suggests a potential successful leaching process, as lower concentrations post-leaching may indicate the removal of Y from the soil. However, the absence of detectable REEs in the 0.1M ammonium sulfate leaching sample could be attributed to the initial low concentration of REEs, emphasizing the importance of considering the baseline concentrations when evaluating leaching efficiency. Conversely, the notable increase in Scandium (Sc) and Ytterbium (Yb) concentrations in the 0.5M leached sample (0.0264% and 0.0019%, respectively) raises intriguing questions. This unexpected rise may be linked to complex interactions between the leaching agent and soil matrix, influencing the release and retention of specific REEs. The observed changes underscore the need for a more comprehensive understanding of the leaching dynamics and the specific behaviour of individual REEs under varying leaching conditions.

This thorough comparative analysis provides valuable insight into the impact of leaching on REE concentrations and highlights the complexities of this process, which has implications for the field of rare earth element extraction from soils.

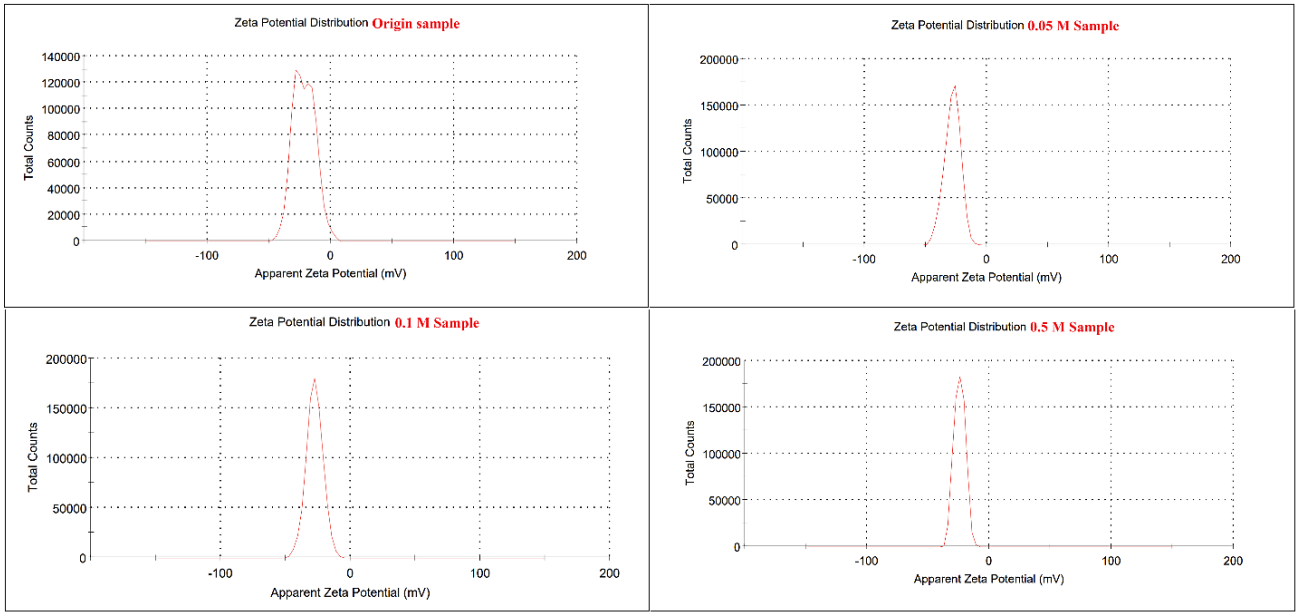

Figure 9: Zeta potential distribution for all samples

3.3. Zeta Potential Test Analysis of Leached Samples

Figure 9 illustrates the zeta potential distribution of the soil samples, including the original sample and those leached with three different concentrations: 0.05M, 0.1M, and 0.5M. The graph represents the average values obtained from a combination of three runs. This distribution graph displays the total counts of zeta potential plotted against the apparent zeta potential. For the original sample, the calculated zeta potential was -21.6 mV, with a standard deviation of 8.93 mV. A high standard deviation implies a lack of consistency or uniformity in the soil sample. This variation may arise from the mixing of soil samples from different areas, even if they share the same depth and site. Variations in mineral composition among samples from different boreholes can lead to a high degree of deviation in the zeta potential counts.

In the case of samples leached with 0.05M ammonium sulfate, the zeta potential exhibited a single peak at -28.1 mV, corresponding to the average zeta potential. The zeta potential deviation was 6.37 mV, which, considering the soil's complex mineral composition, was within the expected range. Similarly, for samples leached with 0.1M ammonium sulfate, the zeta potential displayed a single peak at -27.6 mV, consistent with the average zeta potential. The zeta potential deviation was 6.18 mV, which, again, was in line with expectations given the diverse mineral content of the soil sample. In the case of samples leached with 0.5M ammonium sulfate, the zeta potential exhibited a single peak at -24.1 mV, corresponding to the average zeta potential. The zeta potential deviation was 4.48 mV, a value that aligns with the anticipated variations stemming from the soil's mineral diversity.

The system can be considered stable, as indicated by the high absolute value of zeta potential. This suggests that the attractive forces among surface particles are sufficiently strong to maintain the separation of liquid and surface particles, thus preventing aggregation. However, the soil system remains susceptible to aggregation due to its zeta potential value of less than 30mV (in absolute terms). The presence of certain elements can potentially reduce the zeta potential. Moreover, excessive dispersion in the particles, while favorable in a solution, may have adverse consequences in a soil sample, as it increases the risk of landslides.

Figure 10 presents a histogram depicting the comparison of zeta potential values before leaching and after exposure to three distinct ammonium sulfate concentrations: 0.05M, 0.1M, and 0.5M. An observable increase in zeta potential values is evident after the leaching pro-

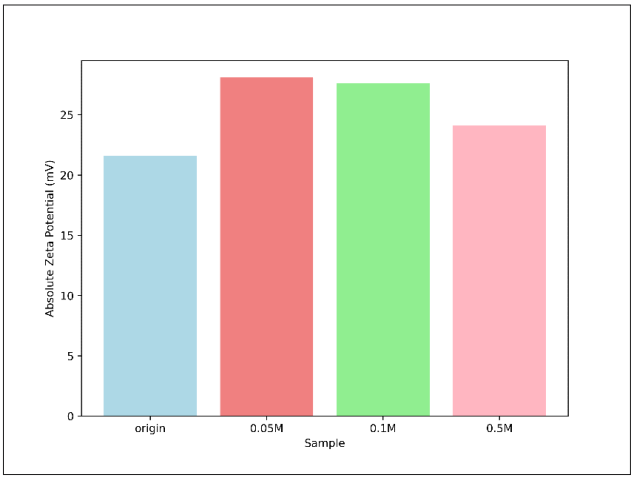

Figure 10: Comparison of zeta potential for different leaching reagent concentrations

Table 6: Liquid limit testing data analysis of different samples

Sample No	Origin Sample		Leached by 0.05M		Leached by 0.1M		Leached by 0.5M	
	Cone Reading (mm)	Moisture Content (%)	Cone Reading (mm)	Moisture Content (%)	Cone Reading (mm)	Moisture Content (%)	Cone Reading (mm)	Moisture Content (%)
1	13.00	25.74	10.8	9.56	12.5	7.77	8.0	3.73
2	16.30	27.09	11.2	3.02	16.7	8.26	15.9	6.12
3	17.70	28.68	18.5	8.84	16.0	10.06	29.1	14.63
4	24.00	27.61	29.8	21.88	25.7	17.83	29.0	17.29
5	32.20	30.71	31.5	24.11	28.8	18.57	33.7	19.95

cess. This increase can be attributed to the potential removal of salts from the soil, along with the introduction of additional negative ions, particularly the ammonium ion. These alterations contribute to enhanced repulsion between soil particles, consequently resulting in an elevated zeta potential.

However, it is worth noting that as the concentration of ammonium ions in the sample increases, there is a greater likelihood of these ions interacting with other elements to form salt compounds. This interaction subsequently reduces the overall zeta potential, as there are fewer negative ions available in the sample.

3.4. Liquid Limit Test Analysis of Leached Samples

Table 6 provides a comprehensive overview of cone readings and moisture content measurements for soil samples, including the original sample, as well as samples leached with 0.05M, 0.1M, and 0.5M ammonium sulfate solutions. Cone readings represent the depth of cone penetration, calculated as the difference between the final reading and the initial reading, while moisture content values exclude the weight of the petri dish. For the original (unleached) samples, cone readings ranged from 13.00 mm to 32.20 mm, and the corresponding moisture content values varied between 25.74% and 30.71%.

In the case of samples leached with 0.05M ammonium sulfate, cone readings were recorded in the range of 10.80 mm to 31.50 mm. The associated moisture content values were observed to be in the range of 3.02% to 24.11%. Similarly, samples leached with 0.1M ammonium sulfate exhibited cone readings ranging from 12.5 mm to 28.80 mm, with moisture content values spanning from 7.77% to 18.57%. For samples leached with 0.5M ammonium sulfate, cone readings ranged from 8.00 mm to 33.70 mm, and the corresponding moisture content values varied between 3.73% and 19.95%.

In addition, **Figure 11** depicts a comparative analysis of liquid limit values for both the original soil sample and the samples subjected to leaching with different concentrations of ammonium sulfate. Notably, there is a consistent downward trend in liquid limit values as the leaching concentration increases. Specifically, the liquid limit values for the original sample, 0.05M sample, 0.1M sample, and 0.5M sample are 27.83%, 13.17%, 12.54%, and 10.32%, respectively.

This trend can be attributed to the influence of ammonium ions introduced during the leaching process, which impacts the soil's flocculation and dispersion behaviour. With an increasing concentration of ammonium ions, there is a greater likelihood of promoting flocculation, leading to the formation of larger soil aggregates.

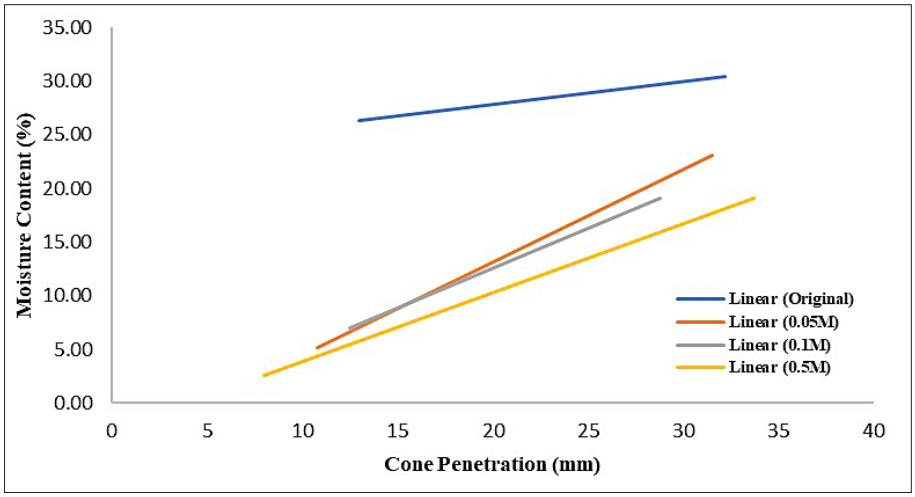

Figure 11: Comparison of various liquid limit

Consequently, this results in a further reduction in the liquid limit values.

3.5. Plastic Limit Test Analysis of Leached Samples

Figure 12 illustrates a comparison of plastic limit values across various soil samples. Notably, the original sample exhibits the highest plastic limit, measuring at 34.34%. However, the impact of the leaching process becomes evident as there is a sharp decrease in plastic limit with increasing concentrations of the leaching reagent.

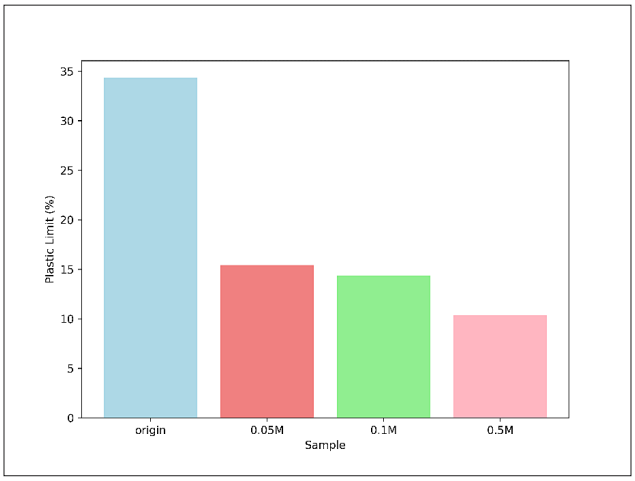

Figure 12: Comparison of plastic limit of different sample

Leaching with lower concentrations, specifically 0.05M and 0.1M, consistently results in an average reduction of approximately 56.59% in plastic limit. In contrast, leaching with a higher concentration of 0.5M leads to a more substantial decrease of around 69.84% in plastic limit. This significant decrease in plastic limit is attributed to the dispersion of clay particles in the soil due to the presence of ammonium sulfate. As clay particles disperse, they lose their ability to bind together, consequently reducing the soil's plasticity. The extent of this reduction in plasticity is directly proportional to the concentration of the leaching reagent.

3.6. Plasticity Index Analysis of Leached Samples

Table 7 presents the plasticity index values for both the original soil sample and the leached samples. The original sample exhibits the highest plasticity index, with a value of 6.51%. In contrast, all leached samples show relatively low plasticity index values. Specifically, the plasticity index for the 0.05M, 0.1M, and 0.5M leached samples is 2.26%, 1.84%, and 0.04%, respectively.

Table 7: Plasticity index analysis of different samples

Sample	Liquid Limit (%)	Plastic Limit (%)	Plasticity Index (%)	Soil Classification
Original	27.83	34.34	6.51	Poor
0.05M	13.17	15.43	2.26	Fair
0.1M	12.54	14.38	1.84	Fair
0.5M	10.32	10.36	0.04	Good

The decrease in the plasticity index values after the leaching process indicates that the soil becomes less plastic in nature compared to the original sample. The classification of the soil is based on subgrade soil classification criteria outlined in (**Naeini and Yousefzadeh, 2023**).

4. Discussion

The comprehensive investigation detailed in this study delves into the intricate interplay between in-situ leaching (ISL) with ammonium sulfate and the mechanical properties of soil. The implications of this research extend beyond a theoretical understanding, bearing significant real-world relevance, especially in regions where rare earth element (REE) extraction via ISL is becoming increasingly prevalent. The findings emphasize the need for a deeper comprehension of the environmental and soil stability impacts of ISL activities, particularly in the context of REE mining.

The research unequivocally demonstrates that ISL leaching with ammonium sulfate has a substantial weakening effect on soil shear strength. The reduction in shear strength across varying leaching concentrations and normal stresses is particularly noteworthy. This outcome implies a higher susceptibility to slope failures, posing a significant concern for areas where ISL operations occur. The reduced shear strength can result in landslides, which are not only environmentally destructive but also represent potential safety hazards for nearby communities.

It is crucial to recognize that the decrease in shear strength is not uniform across all leaching conditions, with the 0.5M concentration displaying a noticeable exception due to potential compaction issues. However, this non-uniformity emphasizes the complexity of ISL's effects on soil mechanical properties, indicating that the outcome depends on multiple factors, including the leaching concentration and the initial soil characteristics.

The research uncovers another vital aspect of soil behaviour altered by ISL activities: plasticity. The reduction in the liquid limit and plastic limit values after leaching points to a decline in soil plasticity. This has implications for soil workability and deformation characteristics. A less plastic soil is more susceptible to cracking and exhibits decreased deformability, which can pose challenges in various construction and engineering applications.

The identification of rare earth elements (REEs), particularly yttrium, through X-ray fluorescence (XRF) analysis adds another layer of complexity to the ISL process. The presence of REEs in the soil, along with specific mineral phases such as Indium Yttrium Antimony Sulfide, underscores the potential environmental consequences of ISL activities. This finding necessitates further investigation into the behaviour of REEs during

ISL, including their mobility, leachability, and long-term environmental impact.

Zeta potential testing provides critical insight into soil stability. The increased repulsion between soil particles post-leaching highlights the potential for soil failure under external forces. While a high zeta potential indicates a stable system, the study reveals that soil can remain prone to aggregation if the absolute zeta potential is less than 30mV. This observation emphasizes the need for a holistic approach to assess the soil's stability under the influence of leaching activities.

It is important to note that conducting laboratory experiments and collecting accurate data on soil mechanical properties can be a complex and time-consuming process. Factors such as sample collection, sample preparation, and testing procedures can introduce potential sources of error or variability in the data. Additionally, the availability of suitable soil samples from rare-earth mines with ion-adsorption characteristics may also pose challenges in terms of accessibility and representativeness. It is crucial for researchers to carefully design their experiments, follow standardized testing protocols, and consider the limitations and uncertainties associated with the data collected.

5. Conclusion

This research illuminates the multifaceted impacts of ISL leaching with ammonium sulfate on soil mechanical properties. The reduction in shear strength, liquid limit, and plastic limit post-leaching underscores the soil's increased vulnerability to slope failures. XRD analysis identifies key mineral phases, with Indium Yttrium Antimony Sulfide emerging as dominant. The presence of REEs, particularly yttrium, detected through XRF, further accentuates the need for scrutinizing the environmental consequences of ISL. The direct shear box test exemplifies the sensitivity of shear stress to normal stresses and leaching concentrations, with cohesion values showing varying patterns. Zeta potential testing underscores the enhanced repulsion between soil particles post-leaching, accentuating the potential for soil failure under external forces. The reduction in liquid limit and plastic limit signifies a diminished soil plasticity. These findings shed light on the intricate interplay between ISL and soil properties, crucial as REE mining via ISL gains traction worldwide. Key results and findings from the research are highlighted as follow:

- The shear strength of the soil decreases after leaching, making it weaker and more susceptible to slope failure.
- The liquid limit of the soil decreases with increasing leaching concentrations, indicating improved workability and reduced plasticity.
- Leaching reduces the plastic limit of the soil, indicating a decreased ability to deform without cracking.
- XRD analysis identified the presence of various mineral phases, including Illite, Indium Yttrium Antimony Sulfide, and Thulium Thorium Iodide.
- XRF analysis confirmed the presence of rare earth elements (REEs) in the soil, with Yttrium being the most significant element detected.
- Zeta potential testing revealed increased repulsion between soil particles after leaching, indicating a potential for soil failure under force.

6. References

Agency, I. A. E. (2005): Guidebook on Environmental Impact Assessment for in Situ Leach Mining Projects. The Agency.

Asahina, D., Pan, P., Tsusaka, K., Takeda, M., and Bolander, J. E. (2018): Simulating hydraulic fracturing processes in laboratory-scale geological media using three-dimensional TOUGH-RBSN. Journal of Rock Mechanics and Geotechnical Engineering, 10(6), 1102-1111. https://doi.org/10.1016/j.jrmge.2018.09.001

Borst, A. M., Smith, M. P., Finch, A. A., Estrade, G., Villanova-de-Benavent, C., Nason, P., Marquis, E., Horsburgh, N. J., Goodenough, K. M., and Xu, C. (2020): Adsorption of rare earth elements in regolith-hosted clay deposits. Nature communications, 11(1), 4386. https://doi.org/10.1038/s41467-020-17801-5

Cai, Z., Wang, F., Gao, C., He, N., Liu, X., Gong, B., Wu, Q., Li, P., Hu, Z., and Ling, H. (2019): Standard for geotechnical testing method. In: China Planning Press: Beijing, China.

Chen, H., Chen, H., Kardos, L., and Szabó, V. (2023): Application of Biochar for Ion-Adsorption of Rare Earth Contaminated Soil Remediation: A Review. Sustainability, 15(10), 7934. https://doi.org/10.3390/su15107934

Chen, Z., Zhang, Z., and Chi, R. (2020): Leaching process of weathered crust elution-deposited rare earth ore with formate salts. Frontiers in Chemistry, 8, 598752. https://doi.org/10.3389/fchem.2020.598752

Chen, Z., Zhang, Z., Liu, D., Chi, X., and Chen, W. (2020): Swelling of clay minerals during the leaching process of weathered crust elution-deposited rare earth ores by magnesium salts. Powder technology, 367, 889-900. https://doi.org/10.1016/j.powtec.2020.04.008

Deng, Z., Qin, L., Wang, G., Luo, S., Peng, C., and Li, Q. (2019): Metallogenic process of ion adsorption REE ore based on the occurrence regularity of La in kaolin. Ore Geology Reviews, 112, 103022. https://doi.org/10.1016/j.oregeorev.2019.103022

Dieterich, J. H., and Conrad, G. (1984): Effect of humidity on time-and velocity-dependent friction in rocks. Journal of Geophysical Research: Solid Earth, 89(B6), 4196-4202. https://doi.org/10.1029/JB089iB06p04196

Dushyantha, N., Batapola, N., Ilankoon, I., Rohitha, S., Premasiri, R., Abeysinghe, B., Ratnayake, N., and Dissanayake, K. (2020): The story of rare earth elements (REEs): Occurrences, global distribution, genesis, geology, mineralogy and global production. Ore Geology Reviews, 122, 103521. https://doi.org/10.1016/j.oregeorev.2020.103521

Feng, J., Wu, X., Gao, Z., Sun, W., Zhou, F., and Chi, R. (2023): Leaching Behavior of Rare Earth Elements and Aluminum from Weathered Crust Elution-Deposited Rare Earth Ore with Ammonium Formate Inhibitor. Minerals, 13(10), 1245. https://doi.org/10.3390/min13101245

Feng, X. T., Li, S. J., and Chen, S. L. (2004): Effect of water chemical corrosion on strength and cracking characteristics of rocks-a review. Key Engineering Materials, 261, 1355-1360. https://doi.org/10.4028/www.scientific.net/KEM.261-263.1355

Fu, W., Luo, P., Hu, Z., Feng, Y., Liu, L., Yang, J., Feng, M., Yu, H., and Zhou, Y. (2019): Enrichment of ion-exchangeable rare earth elements by felsic volcanic rock weathering in South China: Genetic mechanism and formation preference. Ore Geology Reviews, 114, 103120. https://doi.org/10.1016/j.oregeorev.2019.103120

Guo, Z., Zhou, J., Xu, H., Zhou, K., and Jin, J. (2022): Reviews of ionic type rare earth orebody strength weakening and landslide under ore leaching. Chin Rare Earths, 43, 9-22.

Hampton, J., Gutierrez, M., Matzar, L., Hu, D., and Frash, L. (2018): Acoustic emission characterization of microcracking in laboratory-scale hydraulic fracturing tests. Journal of Rock Mechanics and Geotechnical Engineering, 10(5), 805-817. https://doi.org/10.1016/j.jrmge.2018.03.007

He, W., Chen, Z., Shi, H., Liu, C., and Li, S. (2021): Prediction of acoustic wave velocities by incorporating effects of water saturation and effective pressure. Engineering Geology, 280, 105890. https://doi.org/10.1016/j.enggeo.2020.105890

Huang, X.-W., Long, Z.-Q., Wang, L.-S., and Feng, Z.-Y. (2015): Technology development for rare earth cleaner hydrometallurgy in China. Rare Metals, 34, 215-222. https://doi.org/10.1007/s12598-015-0473-x

Izadi, G., and Elsworth, D. (2015): The influence of thermal-hydraulic-mechanical-and chemical effects on the evolution of permeability, seismicity and heat production in geothermal reservoirs. Geothermics, 53, 385-395. https://doi.org/10.1016/j.geothermics.2014.08.005

Kazemi, M. M. K., Nabavi, Z., and Armaghani, D. J. (2023a): A novel Hybrid XGBoost Methodology in Predicting Penetration Rate of Rotary Based on Rock-Mass and Material Properties. Arabian Journal for Science and Engineering, 1-17. https://doi.org/10.1007/s13369-023-08360-0

Kazemi, M. M. K., Nabavi, Z., and Khandelwal, M. (2023b): Prediction of blast-induced air overpressure using a hybrid machine learning model and gene expression programming (GEP): A case study from an iron ore mine. AIMS Geosciences, 9(2), 357-381. https://doi.org/10.3934/geosci.2023019

Kazemi, M. M. K., Nabavi, Z., Rezakhah, M., and Masoudi, A. (2023c): Application of XGB-based metaheuristic techniques for prediction time-to-failure of mining machinery. Systems and Soft Computing, 5, 200061. https://doi.org/10.1016/j.sasc.2023.200061

Li, F.-b., Sheng, J.-c., Zhan, M.-l., Xu, L.-m., Qiang, W., and Jia, C.-l. (2014): Evolution of limestone fracture permeability under coupled thermal, hydrological, mechanical, and chemical conditions. Journal of Hydrodynamics, Ser. B, 26(2), 234-241. https://doi.org/10.1016/S1001-6058(14)60026-3

Li, H., Zhong, Z., Eshiet, K. I.-I., Sheng, Y., Liu, X., and Yang, D. (2020): Experimental investigation of the permeability and mechanical behaviours of chemically corroded limestone under different unloading conditions. Rock Mechanics and Rock Engineering, 53, 1587-1603. https://doi.org/10.1007/s00603-019-01961-y

Li, M., Wang, D., and Shao, Z. (2020): Experimental study on changes of pore structure and mechanical properties of sandstone after high-temperature treatment using nuclear magnetic resonance. Engineering Geology, 275, 105739. https://doi.org/10.1016/j.enggeo.2020.105739

Lin, Y., Zhou, K., Li, J., Ke, B., and Gao, R. (2020): Weakening laws of mechanical properties of sandstone under the effect of chemical corrosion. Rock Mechanics and Rock Engineering, 53, 1857-1877. https://doi.org/10.1007/s00603-019-01998-z

Miao, S., Cai, M., Guo, Q., Wang, P., and Liang, M. (2016): Damage effects and mechanisms in granite treated with acidic chemical solutions. International Journal of Rock Mechanics and Mining Sciences, 88, 77-86. https://doi.org/10.1016/j.ijrmms.2016.07.002

Moldoveanu, G. A., and Papangelakis, V. G. (2012): Recovery of rare earth elements adsorbed on clay minerals: I. Desorption mechanism. Hydrometallurgy, 117, 71-78. https://doi.org/10.1016/j.hydromet.2012.02.007

Moldoveanu, G. A., and Papangelakis, V. G. (2013): Recovery of rare earth elements adsorbed on clay minerals: II. Leaching with ammonium sulfate. Hydrometallurgy, 131, 158-166. https://doi.org/10.1016/j.hydromet.2012.10.011

Nabavi, Z., Mirzehi, M., Dehghani, H., and Ashtari, P. (2023a): A hybrid model for back-break prediction using XGBoost machine learning and metaheuristic algorithms in Chadormalu iron mine. Journal of Mining and Environment, 14(2), 689-712. https://doi.org/10.22044/jme.2023.12796.2323

Nabavi, Z., Mousavi, A., Mirzehi Kalate Kazemi, M., and Monjezi, M. (2023b): Incorporating grade uncertainty into open-pit long-term production planning using loss and profit functions. International Journal of Mining and Geo-Engineering. https://doi.org/10.22059/ijmge.2023.360143.595072

Naeini, S., and Yousefzadeh, M. (2023): Effect of plasticity index and reinforcement on the CBR value of soft clay. In New Horizons in Earth Reinforcement (pp. 335-339). CRC Press.

Nie, W., Zhang, R., He, Z., Zhou, J., Wu, M., Xu, Z., Chi, R., and Yang, H. (2020): Research progress on leaching technology and theory of weathered crust elution-deposited rare earth ore. Hydrometallurgy, 193, 105295. https://doi.org/10.1016/j.hydromet.2020.105295

Saadatkhah, N., Kassim, A., Siat, Q. A., and Micallef, A. (2023): Salt leaching by freshwater and its impact on seafloor stability: An experimental investigation. Marine Geology, 455, 106959. https://doi.org/10.1016/j.margeo.2022.106959

Shang, D., Zhao, Z., Dou, Z., and Yang, Q. (2020): Shear behaviors of granite fractures immersed in chemical solutions. Engineering Geology, 279, 105869. https://doi.org/10.1016/j.enggeo.2020.105869

Shu, B., Zhu, R., Zhang, S., and Dick, J. (2019): A qualitative prediction method of new crack-initiation direction during hydraulic fracturing of pre-cracks based on hyperbolic failure envelope. Applied Energy, 248, 185-195. https://doi.org/10.1016/j.apenergy.2019.04.151

Stockdale, A., and Banwart, S. A. (2021): Recovery of technologically critical lanthanides from ion adsorption soils. Minerals Engineering, 168, 106921. https://doi.org/10.1016/j.mineng.2021.106921

Wang, H., Wang, X., Li, G., Ye, H., Zhang, C., and Zhou, L. (2023a): Weakening of mechanical parameters of ion-absorbed rare-earth ores subjected to leaching. Geomechanics and Geophysics for Geo-Energy and Geo-Resources, 9(1), 124. https://doi.org/10.1007/s40948-023-00661-w

Wang, H., Wang, X., Wang, Y., Wang, D., Hu, K., Zhong, W., and Guo, Z. (2023b): Influence of ammonium sulfate leaching agent on engineering properties of weathered crust elution-deposited rare earth ore. Acta Geotechnica, 1-22. https://doi.org/10.1007/s11440-023-01999-x

Wang, L., Wang, C., Li, L., and Yang, Y.-M. (2018): Readsorption of rare earth elements during leaching process of ion-adsorption-type rare earth ore. Rare Metals, 1-8. https://doi.org/10.1007/s12598-018-1162-3

Wang, X., Wang, H., Sui, C., Zhou, L., Feng, X., Huang, C., Zhao, K., Zhong, W., and Hu, K. (2020): Permeability and adsorption–desorption behavior of rare earth in laboratory leaching tests. Minerals, 10(10), 889. https://doi.org/10.3390/min10100889

Xie, S., Shao, J., and Xu, W. (2011): Influences of chemical degradation on mechanical behaviour of a limestone. International Journal of Rock Mechanics and Mining Sciences, 48(5), 741-747. https://doi.org/10.1016/j.ijrmms.2011.04.015

Yang, L., Wang, D., Li, C., Sun, Y., Zhou, X., and Li, Y. (2018): Searching for a high efficiency and environmental benign reagent to leach ion-adsorption rare earths based on the zeta potential of clay particles. Green Chemistry, 20(19), 4528-4536. https://doi.org/10.1039/C8GC01569D

Yang, M., Liang, X., Ma, L., Huang, J., He, H., and Zhu, J. (2019): Adsorption of REEs on kaolinite and halloysite: A link to the REE distribution on clays in the weathering crust of granite. Chemical Geology, 525, 210-217. https://doi.org/10.1016/j.chemgeo.2019.07.024

Yang, X. J., Lin, A., Li, X.-L., Wu, Y., Zhou, W., and Chen, Z. (2013): China's ion-adsorption rare earth resources, mining consequences and preservation. Environmental Development, 8, 131-136. https://doi.org/10.1016/j.envdev.2013.03.006

Yu, Y., Zhu, W., Li, L., Wei, C., Yan, B., and Li, S. (2020): Multi-fracture interactions during two-phase flow of oil and water in deformable tight sandstone oil reservoirs. Journal of Rock Mechanics and Geotechnical Engineering, 12(4), 821-849. https://doi.org/10.1016/j.jrmge.2019.09.007

Zhang, Z., He, Z., Yu, J., Xu, Z., and Chi, R. (2016): Novel solution injection technology for in-situ leaching of weathered crust elution-deposited rare earth ores. Hydrometallurgy, 164, 248-256. https://doi.org/10.1016/j.hydromet.2016.06.015

Zhong, W., Ouyang, J., Yang, D., Wang, X., Guo, Z., and Hu, K. (2022): Effect of the in situ leaching solution of ion-absorbed rare earth on the mechanical behavior of basement rock. Journal of Rock Mechanics and Geotechnical Engineering, 14(4), 1210-1220. https://doi.org/10.1016/j.jrmge.2021.12.002

SAŽETAK

Utjecaj izluživanja amonijeva sulfata na adsorpciju iona rijetkih zemalja i mehanička svojstva tla

U pojedinim kineskim regijama terensko izluživanje postalo je važna nedestruktivna metoda za ekstrakciju elemenata rijetkih zemalja. Međutim, nakon incidenta s pojavom klizišta raste zabrinutost zbog utjecaja na okoliš i na stabilnost tla uslijed tih aktivnosti. Ovaj članak prikazuje bit opsežnoga istraživačkog pothvata koji istražuje učinke terenskoga izluživanja amonijeva sulfata, koristeći se koncentracijama od 0,05 M, 0,1 M i 0,5 M, na mehanička svojstva tla. Studija obuhvaća fizičko-kemijska, fizička i mehanička ispitivanja kojima se utvrđuju važne promjene u čvrstoći na smicanje, koheziji, kutu unutarnjega trenja, elektrokinetičkom (zeta) potencijalu, granicama plastičnosti i tečenja te indeksu plastičnosti nakon izluživanja. XRF i XRD analize otkrivaju prisutnost elemenata rijetkih zemalja i karakteristične mineralne faze u uzorcima tla. Općenito, terensko izluživanje izaziva slabljenje tla te izaziva zabrinutost zbog potencijalnih slomova na kosinama i naglašava potrebu za dubljim shvaćanjem utjecaja terenskoga izluživanja na svojstva tla u kontekstu rudarenja elemenata rijetkih zemalja.

Ključne riječi:
terensko izluživanje, mehanička svojstva tla, elementi rijetkih zemalja, izluživanje amonijevim sulfatom, utjecaj na okoliš

Authors' contribution

Amirul Asyraf Mohd Hamka (1) (Undergraduate, mineral resources) developed a methodological approach, prepared the samples, did the tests, provided the results, and prepared the reports. **Meisam Saleki (2)** (PhD, lecturer) initialized the idea, proposed the methodology, supervised the research and tests, analysed the results. **Zohreh Nabavi (3)** (Msc, mining engineering) reviewed literary sources, analysed the data, wrote the draft. **Hesam Dehghani (4)** (PhD, associate professor, mining engineering) reviewed the paper, completion a review of the literature, and analysis of the results.